Density functional study of the Σ3 (111) [10] symmetrical tilt grain boundary in SrTiO3

2001 J. Phys.: Condens. Matter 13 3949

(http://iopscience.iop.org/0953-8984/13/18/305)

INSTITUTE OF PHYSICS PUBLISHING JOURNAL OF PHYSICS: CONDENSED MATTER

J. Phys.: Condens. Matter **13** (2001) 3949–3960 www.iop.org/Journals/cm PII: S0953-8984(01)22446-1

Density functional study of the $\Sigma 3$ (111) $[1\bar{1}0]$ symmetrical tilt grain boundary in $SrTiO_3$

S Hutt, S Köstlmeier[1] and C Elsässer[2]

Max-Planck-Institut für Metallforschung, Seestraße 92, D-70174 Stuttgart, Germany

E-mail: elsae@marvin.mpi-stuttgart.mpg.de (C Elsässer)

Received 2 March 2001

Abstract

Density functional supercell calculations were carried out by a mixed-basis pseudopotential method for the $\Sigma 3$ (111) $[1\bar{1}0]$ symmetrical tilt grain boundary in strontium titanate, $SrTiO_3$, as a prototype planar defect in an electroceramic material. A low grain boundary energy of 0.52 J m^{-2} was obtained. Minor structural relaxations compared to the coincidence site lattice model are obtained close to the grain boundary plane by theory and previous experiment. Within the limits of the rather small supercell model employed in the calculations, the calculated geometric structure agrees well with the experimental one. An analysis of calculated local electron densities of states shows that the perturbation due to the grain boundary is localized in the near vicinity of the boundary plane. From the present results for the small supercell model, there is no evidence for the build-up of a space-charge layer at this highly ordered and undoped twin boundary in $SrTiO_3$.

1. Introduction

The properties of functional ceramics are crucially determined by the ion arrangement at grain boundaries, because the geometric and, concomitantly, the electronic structure at internal interfaces influence the ion mobility along and across the grain boundary. It has been pointed out that dopant segregation occurs most commonly to high-energy grain boundaries, i.e. to interfaces, where the stable bulk ion arrangement is most seriously perturbed (see e.g. the recent review [1] and references therein). Apart from that, the mechanical stability of a usually brittle functional ceramic such as $SrTiO_3$ may also be influenced by the presence of planar defects, which limit the range of possible applications. Fixed structural units, including also half-occupied columns close to the grain boundary, have been proposed for the explanation of

[1] Present address: Institut für Physik–Theoretische Physik III, Technische Universität Chemnitz, D-09107 Chemnitz, Germany.

[2] Author to whom any correspondence should be addressed.

0953-8984/01/183949+12$30.00

the experimental findings for some low-angle grain boundaries. Therefore the determination of structural units and grain boundary energies yields further insight into the functional behaviour of a ceramic material.

In the present study the basic structural motif of the $\Sigma 3$ (111) $[1\bar{1}0]$ symmetrical tilt grain boundary, or $\Sigma 3$ (111) twin boundary, in titanate ceramics of perovskite type is investigated. This grain boundary is characterized by a highly ordered and dense atomic arrangement, almost like that inside the bulk $SrTiO_3$ crystal. Because of this high order it is not susceptible to segregation of impurities or dopants. Nevertheless, it provides an ideal model case for accessing the fundamentals and limits of an atomistic characterization of the interfacial structure and bonding with techniques related to transmission electron microscopy.

The $\Sigma 3$ (111) twin boundary in $SrTiO_3$ has been structurally characterized via high-resolution transmission electron microscopy (HRTEM) by Kienzle *et al* [2,3]. The strain-free boundary is mirror symmetric with a polar plane of composition SrO_3 in the grain boundary core. From the HRTEM experiment as well as from calculations with an empirical shell-model approach, no relative translations $T_{[1\bar{1}0]}$ and $T_{[11\bar{2}]}$ of the adjoining crystals along the directions $[1\bar{1}0]$ and $[11\bar{2}]$ parallel to the grain boundary plane could be determined within the limits of accuracy [3]. With respect to the geometrical coincidence-site-lattice (CSL) model the translation component $T_{[111]}$ perpendicular to the boundary plane exhibited a net expansion of 0.61 Å as derived from HRTEM image simulations and of 0.23 Å from the shell-model calculations. HRTEM image simulations yielded minor ion rearrangements with respect to the CSL structure within a boundary region of 13.5 Å. Major deviations from the CSL model occur for the Ti and the Sr ions located in layers 1, 1′, 2, and 2′ next to the grain boundary layer (plane 0 in figure 1, later). With d(Ti–Ti) = 2.25 Å the Ti ions are too close in the CSL model, compared to the distances d(Ti–Ti) = 3.905 Å and d(Ti–Sr) = 3.382 Å in bulk $SrTiO_3$. Therefore, these Ti ions were observed to relax away from the grain boundary, both in the experiment and in the theoretical investigation. On the other hand, the distance d(Sr–Sr) at the grain boundary is enhanced to 4.52 Å in the CSL-model structure compared to the bulk value of d(Sr–Sr) = 3.905 Å. Nevertheless, a further outward relaxation of the (Sr, O) columns in layers 2 and 2′ is concluded from the projection along the $[1\bar{1}0]$ direction in the HRTEM experiment. In the shell-model calculations these Sr ions relax towards the boundary, whereas the O ions of the (Sr, O) columns retain approximately the distance given by the CSL model. The concomitant misalignment of the ions within the (Sr, O) columns amounts to about 0.7 Å, i.e. it would be detectable if present in the experiment [3].

Similar observations have been made for the analogous $\Sigma 3$ (111) twin boundary in $BaTiO_3$ by HRTEM [4–8]. Here, all three translation components, $T_{[1\bar{1}0]}$, $T_{[11\bar{2}]}$, and $T_{[111]}$, are negligibly small. In the $\Sigma 3$ (111) twin of $BaTiO_3$ the Ti ions are also shifted away from the boundary, compared to the CSL structure, to a distance of 2.70 Å [7]. In contrast to the case for $SrTiO_3$ the (Ba, O) columns are located closer to the mirror plane at 4.32 Å. Despite different translations along [111] the relaxations of the first and second layers next to the grain boundary are virtually identical in the $SrTiO_3$ and $BaTiO_3$ twins. A reduced interlayer distance of about 0.8 Å is obtained, compared to the value of 1.12 Å in the CSL model. Furthermore, this structural motif is in very close agreement with the structure of the hexagonal phase of $BaTiO_3$ [9,10]. Thus, the model chosen here to determine the structural units and the electronic structure of the $\Sigma 3$ (111) twin boundary precisely corresponds to the ion arrangement of the hexagonal phase in titanate ceramics.

In this work, a theoretical *ab initio* technique for quantitative calculations of both atomistic and electronic structures, which previously has successfully given microscopic descriptions of grain boundaries in transition metals [11] and in α-Al_2O_3 [12, 13], is employed to analyse the $\Sigma 3$ (111) twin boundary in $SrTiO_3$. In the following, the essential references and computational

parameters of the computational method are given in section 2. The geometry and energetics of the grain boundary are addressed in section 3, and the theoretical results are compared to experimental HRTEM observations for Σ3 (111) twins in $SrTiO_3$ and $BaTiO_3$. In section 4 the electronic structure at the grain boundary is analysed in terms of projected densities of states and of the spatial density distribution of electrons.

2. Computational method

The single crystal and the twin bicrystal of $SrTiO_3$ were investigated by *ab initio* electronic structure calculations based on the local density functional theory (LDFT) [14–17]. Self-consistent total energies and forces were employed to optimize the geometries of the grain boundary supercell with three-dimensionally periodic boundary conditions (see section 3) [18–21]. Electron densities of states (DOS) and real-space valence electron densities were used to analyse the electronic properties at the grain boundary (see section 4).

The core–valence interactions were described by norm-conserving pseudopotentials [22]. The pseudopotential for O was constructed from atomic valence states in the neutral reference configuration $[He]2s^2 2p^{3.5} 3d^{0.5}$. For the Ti and Sr pseudopotentials, ionic reference configurations Ti^{4+} ($[Ne]3s^2 3p^6$) and Sr^{2+} ($[Ar]4s^2 4p^6$) were employed, and the outermost core shells (3s and 3p for Ti, 4s and 4p for Sr) were incorporated as valence states.

The valence electron Bloch states were represented by a mixed basis including plane waves up to a maximum kinetic energy of $E_{pw} = 25$ Ryd (1 Ryd = 13.606 eV), and atom-centred, localized functions, three with angular p symmetry for O sites, and nine each with s, p, and d symmetries for both Ti and Sr sites. The localized functions are confined to spheres with radii $r_{lo}(O) = 1.9$ Bohr and $r_{lo}(Ti) = r_{lo}(Sr) = 1.6$ Bohr (1 Bohr = 0.529 Å). Brillouin-zone integrals were calculated on a $4 \times 4 \times 2$ Monkhorst–Pack k-point mesh for the grain boundary supercell [23].

Densities of valence electron states were analysed locally by projection onto spheres at the atomic sites (PDOS). The projection radii were adjusted for the $SrTiO_3$ single crystal such that the projection spheres contain the formal ionic charges: $r_{pr}(Sr^{2+}) = 2.61$ Bohr; $r_{pr}(Ti^{4+}) = 1.53$ Bohr; $r_{pr}(O^{2-}) = 2.84$ Bohr. The PDOS were calculated from the energy eigenvalues on the k-point mesh by broadening with a Gaussian function of 0.2 eV width. This width was chosen to produce sufficient detail in the PDOS plots of figures 2–5, later. For a pictorial representation of the electronic structure and bonding at the grain boundary, electron-density difference maps are used, in which a superposition of neutral atomic densities centred at the atom positions in the crystal is subtracted from the grain boundary density. Such maps along two cut planes through the supercell are displayed in figures 6 and 7, later. Bright areas indicate zones of accumulation of electronic charge (O anions) and dark areas correspond to zones of electron depletion (Ti and Sr cations). Eleven equidistant contours are selected in a range from -0.05 electrons $Bohr^{-3}$ to +0.05 electrons $Bohr^{-3}$. The cuts are along the (111) plane directly located at the interface and along a $(1\bar{1}0)$ plane intersecting all three ions.

3. Grain boundary geometry and energetics

The size and the shape of the supercell employed in the present study is indicated by the shaded area in figure 1. It contains two equivalent grain boundaries at a spacing of six (111) lattice planes and three-dimensionally periodic boundary conditions are imposed. This smallest usable supercell model of the Σ3 (111) twin boundary is comprised of six $SrTiO_3$ formula units, or of 30 atoms. It is equivalent to the structure of the hexagonal phase, which has been

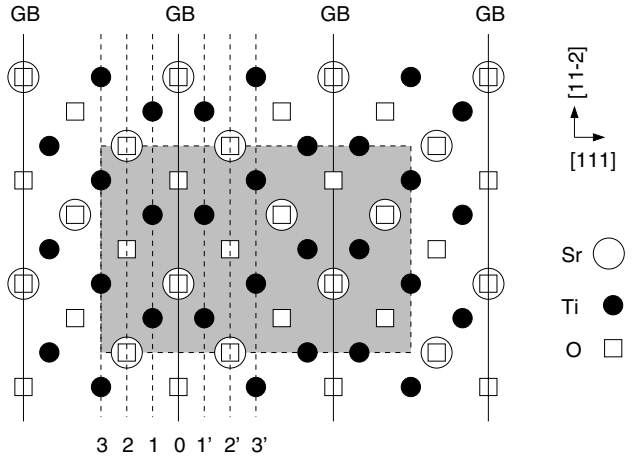

Figure 1. A schematic representation of the supercell model employed for the present study of the $\Sigma 3$ (111) twin boundary. Displayed is the stacking sequence of polar Ti and SrO_3 planes along the [111] direction. The grey shaded area marks the supercell size and shape.

reported for $BaTiO_3$ [10]. This model accounts for the entire region at the grain boundary, in which relevant structural relaxations had been observed by HRTEM [24].

With respect to the mirror twin, no lateral grain translations along $[1\bar{1}0]$ and $[11\bar{2}]$ had been obtained for the strain-free structure of the boundary in the TEM experiments [3]. Our theoretical investigations yielded as well that the grains displaced rigidly along $[1\bar{1}0]$ and $[11\bar{2}]$ away from the mirror-symmetric configuration resulted in energetically unstable configurations. Hence, only the axial grain translation $T_{[111]}$ needed to be optimized for the mirror twin. Structural relaxations of the atom positions in the supercell were determined for several values of $T_{[111]}$. The grain boundary structure with the lowest energy is characterized by an expansion $T_{[111]}$ of 0.16 Å perpendicular to the boundary plane with respect to the CSL model, an enhanced spacing d(Ti–Ti) of 2.63 Å and a contracted distance d(Sr–Sr) of 3.97 Å across the interface.

Table 1 gives a comparison of the calculated structural data, including relaxations, to those of the CSL model, to the experimental data for the $\Sigma 3$ (111) twin boundaries in $SrTiO_3$ [2,3] and $BaTiO_3$ [7], to the $BaTiO_3$ hexagonal phase [10], and to the results of shell-model calculations [3]. Similarly to the shell-model study, the present LDFT results yield a considerably smaller axial translation state $T_{[111]}$, here smaller by a factor of 1/4 than the experimentally derived one [3]. The calculated values resemble more closely the value $T_{[111]} = 0.28$ Å which had been found earlier for a sheared structure of the $\Sigma 3$ (111) twin of $SrTiO_3$ [2]. This sheared structure was observed in a different sample cut from the same bicrystal as the sample with the mirror-symmetric boundary of reference [3]. Concomitantly with $T_{[111]}$, also the calculated distances d(Ti–Ti) and d(Sr–Sr) are smaller than the corresponding values from the HRTEM image simulations of the $\Sigma 3$ (111) twin of $SrTiO_3$ [3]. In fact, the LDFT data are rather close to the experimental distances for $BaTiO_3$, both in the twin [7] and in the hexagonal phase [10], for which no grain boundary expansion was reported.

Despite this difference concerning the axial translation state, the spacing between the cations of the first and the second plane parallel to the interface is contracted to 0.68 Å in rather good agreement with the values of about 0.8 Å obtained by all three experiments [3, 7, 10]. This relaxation is a crucial feature of the grain boundary structure in several respects. First, it is the pathway to a more homogeneous ion redistribution at the boundary, where bulk values

Table 1. Structural properties of the Σ3 (111) twin boundary in $SrTiO_3$ and related planar defects. LDFT(a), LDFT(b), and LDFT(c) are results of the present calculations for the CSL model (a), for the relaxed constant-volume (CV) structure (b), and for the relaxed and expanded structure (c). SM refers to shell-model calculations of reference [3]. TEM(a) and TEM(b) are results for the Σ3 (111) twin of $SrTiO_3$ taken from references [3] and [2], TEM(c) for the Σ3 (111) twin of $BaTiO_3$ from reference [7], and TEM(d) for hexagonal $BaTiO_3$ from reference [10]. In the fifth and sixth columns Ti(1)–Sr(2) and Sr(2)–O(2), only the relevant component parallel to [111] is given. (All translations and spacings are given in Å.)

	$T_{[111]}$	Ti(1)–Ti(1′)	Ti(1)–Sr(2)	Sr(2)–Sr(2′)	O(2)–O(2′)	Sr(2)–O(2)
LDFT(a)	0.00	2.22	1.11	4.43	4.43	0.00
LDFT(b)	0.00	2.58	0.66	3.90	4.46	0.28
LDFT(c)	0.16	2.63	0.68	3.97	4.57	0.30
SM	0.23	2.93	0.11	3.14	3.82	0.34
TEM(a)	0.61	3.2	0.8	4.8	4.8	0.0
TEM(b)	0.28	—	—	—	—	—
TEM(c)	0.00	2.70	0.80	4.32	4.32	—
TEM(d)	0.00	2.67	0.79	4.28	4.28	—

are approached for the ion distances; for instance, d(Sr–Sr) = 3.97 Å (bulk: 3.905 Å). Second, it signifies the shift of formally charged lattice planes, which may provide a driving force for the segregation of impurity ions in a doped electro-ceramic.

In both the present LDFT investigation and the shell-model study [3] the (Sr, O) columns of the second plane parallel to the interface (2 and 2′) dissociate into two columns with Sr and O occupancy, respectively. With 0.30 Å, however, the extent of dissociation obtained by LDFT is only half as large as the one obtained using the shell model [3]. The calculated ion distance d(O–O) = 4.57 Å is rather close to the experimentally derived distance of 4.8 Å with the assumption of non-dissociated SrO columns. This may be an incentive for experimentalists to reinvestigate the influence of atom column dissociation in the HRTEM image simulation, on the basis of the LDFT atomistic structure.

The grain boundary energy obtained for the relaxed and expanded structure amounts to $E_{gb} = 0.52$ J m^{-2}. This energy is much lower than the energy of the most stable, unpolar (001) surface of $SrTiO_3$, which was determined as 1.42 J m^{-2} with the same mixed-basis pseudopotential method [25]. In contrast to the (001) planes, the (111) planes of unperturbed $SrTiO_3$ consist of either (SrO_3) units or Ti atoms (see figure 1), which bear formal charges of 4− and 4+, respectively. Thus, the Σ3 (111) twin boundary of $SrTiO_3$ would have to break up into two polar (111) surfaces. As polar surfaces are usually higher in energy than the unpolar (001) surface, one can conclude from these results that the Σ3 (111) twin is very stable. This is comparable to the case for the very stable rhombohedral Σ7 ($10\bar{1}2$) twin in α-Al_2O_3, which has a similarly low grain boundary energy of 0.63 J m^{-2} [12]. The energy calculated for the Σ3 (111) twin boundary of $SrTiO_3$ with the LDFT is lower than the one obtained from shell-model simulations, the latter amounting to 1.14 J m^{-2}. A similar difference by a factor of about two between LDFT and shell-model interface energies was observed recently as well for the case of the basal Σ3 (0001) twin in α-Al_2O_3 [13].

The CSL structure of the Σ3 (111) twin boundary of $SrTiO_3$ without relaxation or expansion is slightly higher in energy, with 0.78 J m^{-2}. The major energy gain is already obtained by relaxing all atoms in the supercell of the CSL model without any expansion along [111]. This gives a CV relaxed structure with a grain boundary energy of 0.59 J m^{-2}. Hence, in the following discussion of the electronic structure, reference will also be made to this relaxed CV structure.

4. Grain boundary electronic structure

4.1. Projected densities of states

The site- and angular-momentum-projected densities of states of the cationic and anionic sites of bulk $SrTiO_3$ are depicted in figure 2. Typically for an LDFT calculation the band gap is underestimated: 2.3 eV in comparison to the experimental optical energy gap of 3.2 eV [26]. Although the projection radii were chosen to give the formal charges of O^{2-}, Ti^{4+}, and Sr^{2+} in the projection spheres for bulk $SrTiO_3$, there is a noticeable Ti d contribution among the O 2p valence states. Additionally, a signature of the Sr p states is discernible in the O PDOS close to the O 2s states. This indicates that in bulk $SrTiO_3$ the O ions are not ideally spherical, but polarized, especially along the Ti–O bonding direction. The dominant valence bonding contributions are composed of O 2s and 2p, Sr 4p, and Ti 3d states.

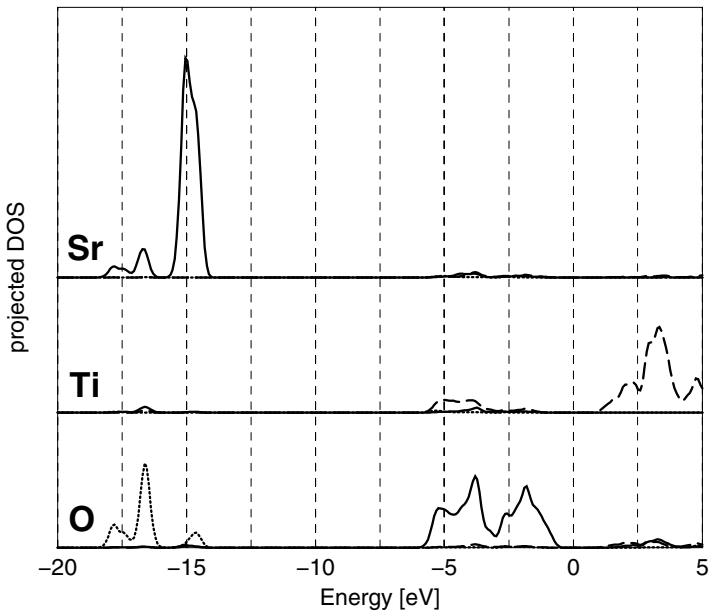

Figure 2. Site- and angular-momentum-projected densities of states at the three different ionic centres in bulk $SrTiO_3$. For better representation the curves for the different elements are depicted on the same scale, but shifted along the *y*-direction. The s-, p-, and d-PDOS are drawn as dotted, continuous, and dashed lines, respectively.

These main features of the bulk electronic structure are compared with those obtained for the ideal CSL model, the relaxed CV structure, and the relaxed and expanded optimum grain boundary structure in figures 3–5. A glance at the PDOS for the different sites shows that the major changes of the PDOS in comparison to the bulk occur due to the ion relaxation at constant volume. As already shown for the grain boundary energy, the expansion plays a rather small role.

Comparing the PDOS curves in more detail, the differences between the (111) planes become obvious. Both the O (figure 3) and the Sr ions (figure 4) in the boundary layer (0) still exhibit a close agreement with the corresponding bulk DOS curves. For the relaxed structures (c) and (d) only a slight increase of the DOS weight close to the Fermi level is obtained. The more pronounced change is monitored for the Sr and O ions of the layers 2, 2′, where the lower

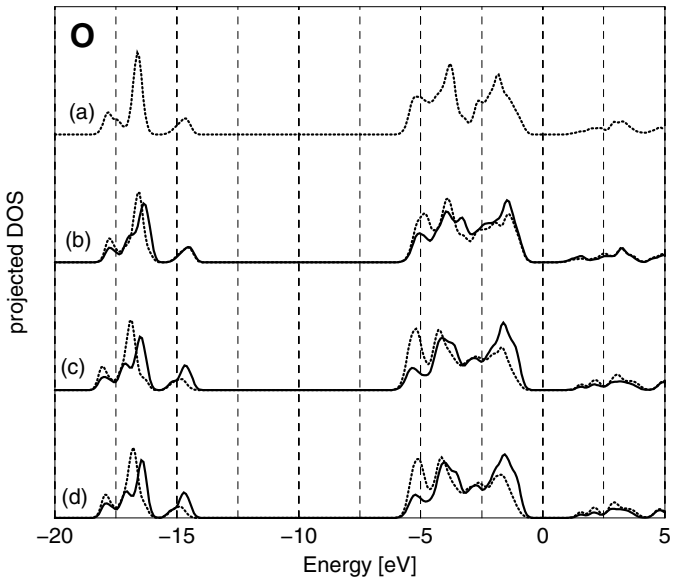

Figure 3. Site-projected DOS of the O ions of (a) bulk $SrTiO_3$, (b) the ideal CSL model, (c) the relaxed CV structure, and (d) the relaxed and expanded structure. Here, and in figures 4 and 5, solid lines refer to PDOS curves of Ti in plane 1, and of Sr and O in plane 0. Dotted lines are PDOS curves of Ti in plane 3, and of Sr and O in plane 2.

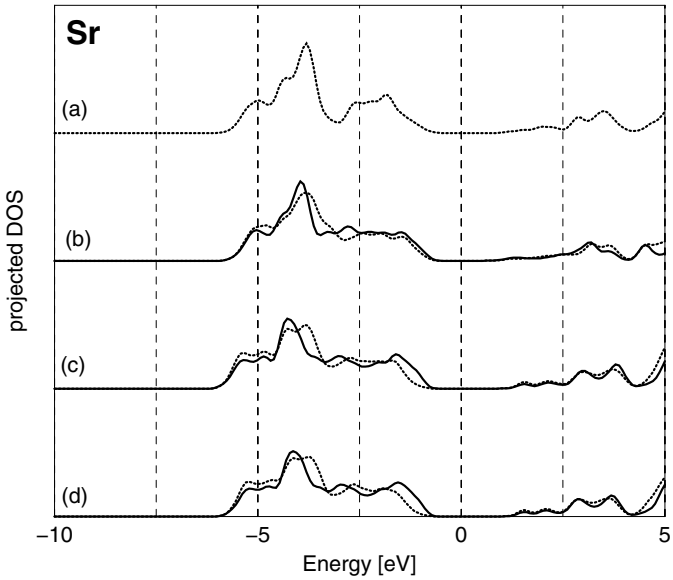

Figure 4. Site-projected DOS of the Sr ions of (a) bulk $SrTiO_3$, (b) the ideal CSL model, (c) the relaxed CV structure, and (d) the relaxed and expanded structure (cf. the caption of figure 3).

edge of the 2p band is gaining weight compared to the upper edge. Along with this, also the O 2s states experience a shift towards stronger binding energies. As this effect becomes most prominent upon ion relaxation, it is probably due to the misalignment of the O and Sr ions

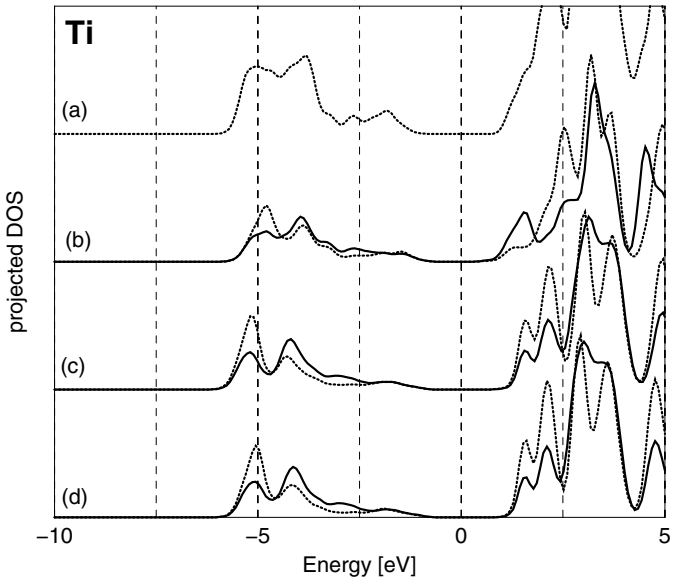

Figure 5. Site-projected DOS of the Ti ions of (a) bulk $SrTiO_3$, (b) the ideal CSL model, (c) the relaxed CV structure, and (d) the relaxed and expanded structure (cf. the caption of figure 3).

within the column along the $[1\bar{1}0]$ direction. Therefore, indications for this dissociation of the (Sr, O) columns might be observable from spectroscopical measurements, which probe local atomic environments.

Both Ti layers experience changes of the PDOS with respect to the bulk (see figure 5). The Ti ions directly located in the first plane next to the grain boundary show a stronger splitting of the lowest unoccupied states, especially for the unrelaxed CSL structure (b) where the ions of layers 1 and $1'$ are closest to each other. Otherwise, the small d contribution to the valence band remains rather bulk-like. The Ti ions of the third layer display traces of their interaction with the O ions of layer 2, where spectral weight was shifted to lower energies below the Fermi level upon relaxation.

On the whole, the band gap is only marginally decreased in the CSL structure, and is recovered again in the relaxed and expanded structure. Hence, as in reference [27] for the $\Sigma 5$ (210) [001] symmetrical tilt grain boundary of $SrTiO_3$, no additional boundary states are present which could influence the ballistic electrical conductivity along the grain boundaries. From the layer-resolved analysis of the PDOS, we conclude that the important changes with respect to bulk $SrTiO_3$ occur in the close vicinity of the grain boundary. The shape of the PDOS of the Ti ions in layer 3, however, yields an indication that our supercell model is rather small and perhaps cannot account for the full structural relaxation.

4.2. Electron-density distribution

Electron-density distribution maps are depicted in figure 6 and figure 7 for two different spatial cuts, one along the Sr, O(111) boundary plane and one in a $(1\bar{1}0)$ plane intersecting all three ions. The electron accumulation at O ions gives rise to the bright contours, the depletion at the Sr and Ti cations to the dark ones. Four panels are given in each figure for (a) the unperturbed bulk, (b) the ideal CSL model, (c) the relaxed CV structure, and (d) the relaxed and expanded structure.

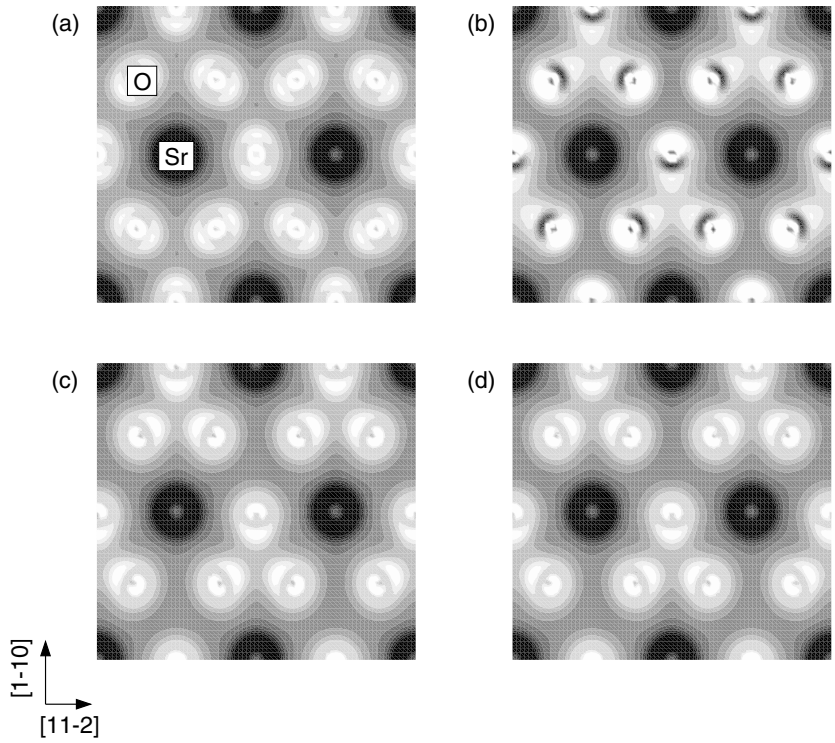

Figure 6. The electron-density difference between the solid and a superposition of free atoms in the grain boundary (111) plane. In order to help with visualizing the effect of the structural relaxation, the redistribution map is shown for (a) bulk $SrTiO_3$, (b) the CSL structure, (c) the relaxed CV structure, and (d) the relaxed and expanded structure.

The map of an Sr, O(111) plane (figure 6) in pure bulk $SrTiO_3$ (a) depicts the hexagonal close-packed structure of this layer clearly. The depletion zone in the near vicinity of the Sr nuclei is spherical, as one would assume in the case of isotropic, purely ionic bonding. Also the outer region exhibits a regular, slightly hexagonal shape. The O anions on the other hand show a less symmetrical pattern, where some directionality of the bonding may be assumed. In reference [27] less of the O fine structure is visible due to the larger spacing of the density difference contours used there.

In the Sr, O(111) grain boundary plane (0) the electron redistribution around the Sr centre distorts to trigonal shape, but no evidence appears that the Sr ions participate other than by ionic interaction. The changes to the O anions are more pronounced. In the CSL structure (b), two Ti cations are located very close to the boundary plane above and below the centre of an O triangle. This heavily distorts the O valence shell in order to shield the strong cation–cation repulsion. Upon structural relaxation, (c) and (d), however, the O triangles contract, and the O valence shells can screen the remaining Ti–Ti repulsion with less deviation from the bulk electron arrangement. Thus, the electron-density redistribution maps give a pictorial representation of the changes observed for the O PDOS at the boundary.

In the cut through a $(1\bar{1}0)$ plane (figure 7) all three ions are present. Again, the Sr ion appears perfectly spherical, whereas the distortions of the O and Ti ions indicate some directionality of the interaction along the Ti–O–Ti bonds. The strongest deviation from the bulk electron arrangement (a) is obtained for the CSL structure (b). In the $(1\bar{1}0)$ plane the pile-up of

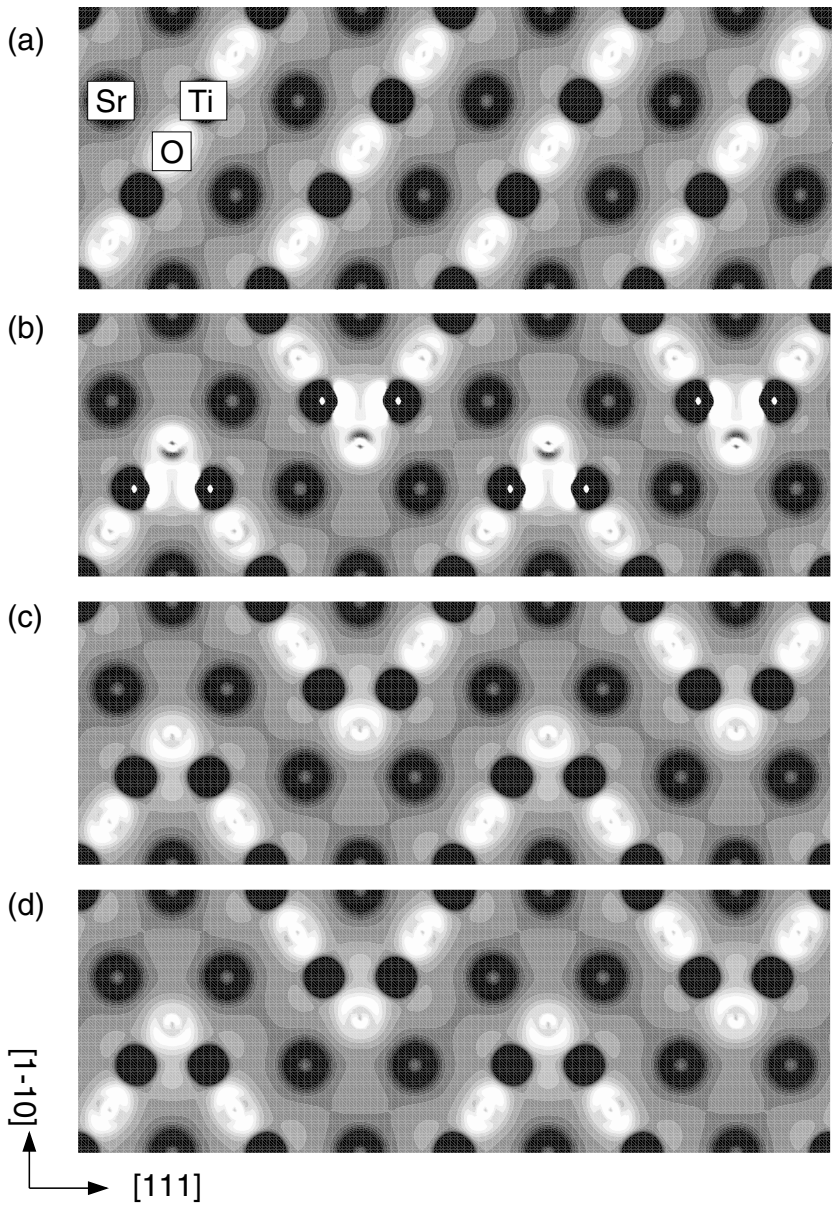

Figure 7. The electron-density difference between the solid and a superposition of free atoms in a $(1\bar{1}0)$ plane intersecting all three ions. To demonstrate the effect of the structural relaxation, the redistribution map is shown for (a) bulk $SrTiO_3$, (b) the CSL structure, (c) the relaxed CV structure, and (d) the relaxed and expanded structure.

electronic charge between the two Ti cations next to the boundary is remarkably pronounced. Both the O anions at the boundary and the Ti cations experience a strong deformation of their respective valence shells. The O ions are no longer polarized along the Ti–O directions, but towards the centre of the short Ti(1)–Ti(1′) distance. The Ti cations are highly non-spherical, and even the O ions of layers 2 or 2′ show some distortion.

After structural relaxation at constant volume, (c), the electronic structure is redistributed to a more bulk-like arrangement. The electron accumulation between the Ti ions of layers 1 and 1′ is considerably reduced due to the increase of the Ti(1)–Ti(1′) distance. Thus, the valence shells of the Ti ions in layers 1 and 1′ regain almost the same shape as in the unperturbed bulk. The O ions in the boundary plane rehybridize along the bent Ti–O–Ti fragment, and the O ions of layer 2 again exhibit an electron arrangement similar to that in the bulk. The additional grain boundary expansion (d) towards the fully optimized structure adds no further significant feature.

From the cut in the $(1\bar{1}0)$ plane there is no evidence for the build-up of a homogeneous space-charge layer close to the grain boundary. For the close-packed, defect-free, and low-energy grain boundary structure, this result is not unexpected. However, as space-charge layers can extend over several lattice planes, caution is needed when interpreting the present results, since they have been obtained with a supercell model of rather small size.

5. Conclusions

Mixed-basis pseudopotential calculations within the local density functional theory were performed in order to determine the structural motif and to analyse the electronic properties of the Σ3 (111) twin boundary in $SrTiO_3$.

The key structural features are an expansion $T_{[111]}$ of 0.16 Å perpendicular to the boundary, an increased Ti–Ti distance of 2.63 Å, and a reduced Sr–Sr distance of 3.97 Å across the grain boundary. The latter two values give rise to a decreased lattice plane spacing of 0.68 Å between the two (111) planes directly adjacent to the grain boundary. The same structural motif has been observed experimentally for the Σ3 (111) twin boundaries in $SrTiO_3$ and in $BaTiO_3$, as well as in hexagonal $BaTiO_3$ with an interplanar spacing of 0.8 Å. Thus, the Sr ions of layers 2 and 2′ try to get close to the bulk distance of d(Sr–Sr) = 3.905 Å. Additionally, the (Sr, O) columns of the second (111) plane adjacent to the boundary dissociate by 0.30 Å to yield an O–O distance of 4.57 Å in the present calculation. This column dissociation was not accounted for in the image simulation of the transmission electron micrograph in reference [3]. The experimentally observed large expansion of 4.8 Å for the Sr(2)–Sr(2′) distance may be connected with this assumption.

The grain boundary energy of the relaxed and expanded structure is very low, namely 0.52 J m^{-2}. Compared to the ideal CSL structure, the major energy gain of 0.19 J m^{-2} (from E_{gb} = 0.78 J m^{-2} of the CSL structure to E_{gb} = 0.59 J m^{-2} of the relaxed CV structure) is obtained already by the relaxation of the ion positions without expansion perpendicular to the grain boundary. This confirms the significance of the structural motif described above. In comparison to the ion relaxation, the energy gain of 0.07 J m^{-2} (from 0.59 J m^{-2} to 0.52 J m^{-2}) due to grain boundary expansion is a minor effect. Considering the low grain boundary energy, the hexagonal phase of $SrTiO_3$ is also a possible, metastable state of the system, unless there exists a reconstruction pathway not investigated in the present study.

The analysis of the calculated electronic structures by means of both projected densities of states (PDOS) and electron-density distribution maps demonstrates that the perturbation caused by the grain boundary is localized within two lattice planes adjacent to the boundary plane. These are precisely the layers involved in the key structural feature described in section 3. Again, the expansion perpendicular to the boundary plane has no significant influence on the PDOS or the electron distribution.

No defect states originating from the Σ3 (111) twin boundary were found in the energy gap between the valence and conduction bands of $SrTiO_3$ by the present calculations. Thus, the boundary does not open up a channel for ballistic electrical conduction along the interface.

Even at the grain boundary the electron depletion around Sr ions retains its spherical shape, which is interpreted as a sign for predominantly ionic interaction with the environment. For Ti and O, on the other hand, the directionality of the O p–Ti d interaction present in the bulk is recovered at the interface by the structural relaxation.

In summary, both the geometric and the electronic structure of the $\Sigma 3$ (111) twin boundary tend to be as close to the values for the pure, unperturbed bulk $SrTiO_3$ as possible. Therefore, no evidence for the occurrence of space-charge layers adjacent to the undoped boundary is obtained from the present LDFT supercell calculations.

Acknowledgments

The authors thank T Gemming for many discussions concerning the TEM experiments and for valuable help in supplying computational resources. They are grateful to M Rühle for his continuous interest and support for this project, and to O Kienzle for his help in the initial stage of the investigation. SK acknowledges stimulating discussions with A Recnik on experimental backgrounds.

References

[1] Waser R and Hagenbeck R 2000 *Acta Mater.* **48** 797
[2] Kienzle O and Ernst F 1997 *J. Am. Ceram. Soc.* **80** 1639
[3] Kienzle O, Exner M and Ernst F 1998 *Phys. Status Solidi* a **166** 57
[4] Recnik A, Bruley J, Mader W, Kolar D and Rühle M 1994 *Phil. Mag.* B **70** 1021
[5] Jia C L, Urban K, Mertin M, Hoffmann S and Waser R 1998 *Phil. Mag.* A **77** 923
[6] Hamada E, Cho W-S and Takayanagi K 1998 *Phil. Mag.* A **77** 1301
[7] Jia C L and Thust A 1999 *Phys. Rev. Lett.* **82** 5052
[8] Jia C L, Rosenfeld R, Thust A and Urban K 1999 *Phil. Mag. Lett.* **79** 99
[9] Burbank R D and Evans H T 1946 *Acta Crystallogr.* **1** 330
[10] Eibl O, Pongratz P and Skalicky P 1987 *Phil. Mag.* B **57** 521
[11] Ochs T, Beck O, Elsässer C and Meyer B 2000 *Phil. Mag.* A **80** 351
[12] Marinopoulos A G and Elsässer C 2000 *Acta Mater.* **48** 4375
[13] Marinopoulos A G, Nufer S and Elsässer C 2001 *Phys. Rev.* B **63** 165112
[14] Hohenberg P and Kohn W 1964 *Phys. Rev.* **136** B864
[15] Kohn W and Sham L J 1965 *Phys. Rev.* **140** A1133
[16] Ceperley D M and Alder B J 1980 *Phys. Rev. Lett.* **45** 566
[17] Perdew J P and Zunger A 1981 *Phys. Rev.* B **23** 5048
[18] Louie S G, Ho K M and Cohen M L 1979 *Phys. Rev.* B **19** 1974
[19] Elsässer C, Takeuchi N, Ho K M, Chan C T, Braun P and Fähnle M 1990 *J. Phys.: Condens. Matter* **2** 4371
[20] Ho K M, Elsässer C, Chan C T and Fähnle M 1992 *J. Phys.: Condens. Matter* **4** 5189
[21] Meyer B, Elsässer C and Fähnle M *Fortran90 Program for Mixed-Basis Pseudopotential Calculations for Crystals* Max-Planck-Institut für Metallforschung, Stuttgart (unpublished)
[22] Vanderbilt D 1985 *Phys. Rev.* B **32** 8412
[23] Monkhorst H and Pack J D 1978 *Phys. Rev.* B **8** 5747
[24] Kienzle O 1999 *Dissertation* Universität Stuttgart
[25] Ochs T, Köstlmeier S and Elsässer C 2001 *Integrated Ferroelectrics* at press
[26] Cardona M 1965 *Phys. Rev.* **140** A651
[27] Mo S-D, Ching W Y, Chisholm M F and Duscher G 1999 *Phys. Rev.* B **60** 2416